(Received 16 April 2025, Accepted 22 May 2025, Scheduled 2 June 2025)

Subwavelength Resonator for the Design of a Waveguide-Fed Metasurface Antenna

Ivan Diaz[1, 2, *], Carlos Arturo Suarez Fajardo[1], Juan Domingo Baena Doello[3], and Hector Guarnizo[2]

[1]Department Engineering, Universidad Distrital F.J.C, Bogotá D.C., Colombia
[2]Department Engineering, Universidad El Bosque, Bogota D.C., Colombia
[3]Department of Physics, Universidad Nacional de Colombia, Bogotá D.C, Colombia

ABSTRACT: Antennas are one of the most important elements in modern communication systems. Recently, significant progress has been made in developing metasurface antennas as an alternative for beam steering, commonly used in radar and communication applications. Metasurface antennas consist of an array of metamaterial elements, uniformly distributed and with subwavelength dimensions, which can be excited by a progressive wave. This work focuses on the application of Incremental Difference Method for estimating the magnetic polarizability of metamaterial arrays embedded in a waveguide-fed linear configuration. The method is validated through full-wave simulations and further assessed using a weighting function introduced in prior studies. The design is demonstrated using a WR340 waveguide-based metasurface antenna model.

1. INTRODUCTION

Metasurface antennas (MSAs) represent an advanced class of antennas that utilize metasurfaces to efficiently control and manipulate electromagnetic waves. Metasurfaces are ultra-thin artificial structures composed of subwavelength elements — smaller than the wavelength of the electromagnetic radiation they interact with — which allow precise modification of the amplitude, phase, and polarization of electromagnetic waves. These properties enable metasurface antennas to adjust wave characteristics with high precision, providing customizable radiation patterns and controlled beam directionality [1]. Their lightweight and low-profile design makes them ideal for integration into flat surfaces, such as those on vehicles or buildings [2]. Furthermore, MSAs are highly efficient and reconfigurable, playing a critical role in technologies such as 5G/6G communications, radar imaging, and portable devices, offering a wide range of functionalities [3].

The growing relevance of metasurface antennas is reflected in the increasing body of research, with numerous studies highlighting their applications in 5G/6G, wireless communications, and radar systems [4–7]. Key areas of focus in these studies include the dynamic reconfiguration of radiation patterns, improved efficiency, and the integration of metasurfaces into high-frequency technologies [8]. Metasurface antennas have gained considerable attention due to their ability to control electromagnetic waves at subwavelength scales. Recent reviews, such as [9], comprehensively discuss state-of-the-art developments, including dynamic beam steering and high-efficiency implementations.

This work contributes to the advancement of waveguide-fed metasurface antennas by combining a localized polarizability extraction technique — based on the Incremental Difference Method — with a realistic waveguide excitation model. Unlike previous studies that rely on idealized excitation conditions or assume continuous weighting functions, our method accounts for the physical constraints of subwavelength resonant elements and guides the design of amplitude and phase profiles within these limitations. This provides a practical path toward compact, steerable antennas for next-generation radar and communication systems.

In this paper, we present the design and validation of a metasurface antenna based on Complementary Electric-LC (CELC) structures [10, 11], excited through a WR340 waveguide-fed system. The antenna structure comprises three main sections: a coaxial-to-waveguide adapter, a separating section, and a short-circuited termination. Section 2 introduces the theoretical framework of the design, grounded on classical Lorentz theory and the extraction of single-port polarizability. Section 3 focuses on validating the Incremental Difference Method, which enables the characterization of the metamaterial cell response at different positions along the waveguide. Subsequently, the implementation of phase control is examined using Lorentzian Constrained Phase Hologram (LCPH) method proposed in [12], leveraging the available amplitude and phase information for each metamaterial element. Finally, in Section 4, the design is validated through full-wave simulations using a model that closely resembles a practical implementation.

2. THEORETICAL MODEL

Any element that can distribute charges by electric or magnetic effects has a polarizability. This concept defines the ability to form instantaneous dipoles in dynamic response to external fields. Metamaterials do not possess an inherent property

* Corresponding author: Ivan Eduardo Diaz Pardo (iediaz@unbosque.edu.co).

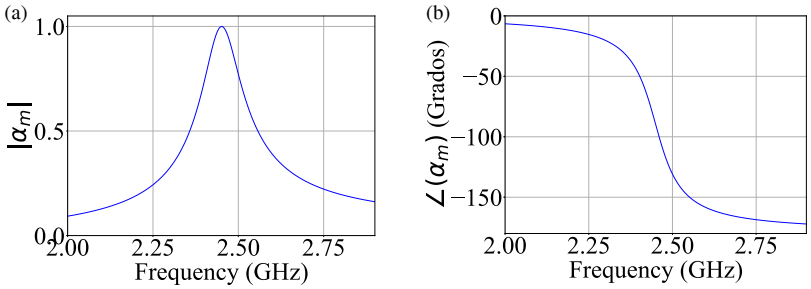

FIGURE 1. Analytical response of a metamaterial unit cell based on Lorentzian polarizability. (a) Magnitude $|\alpha|$ versus frequency, (b) Phase $\angle\alpha$. versus frequency.

of polarizability, and based on the theory of polarizability of molecules it is possible to obtain a relationship between the dipole moment **p** and **m** and the electric and magnetic fields, respectively. The response of each dipole can be described by the polarizability tensor relating incident electric field.

$$\mathbf{p} = \epsilon_0 \hat{\alpha}_e \mathbf{E}^+ = \epsilon_0 \alpha_e \mathbf{E}_{loc} \quad (1)$$

$$\mathbf{m} = \hat{\alpha}_m \mathbf{H}^+ = \alpha_m \mathbf{H}_{loc} \quad (2)$$

Equations (1) and (2) indicate that the electric dipole moment **p** and magnetic dipole moment **m** in a metamaterial structure are induced by both the external fields $\mathbf{E}^+$ and $\mathbf{H}^+$, as well as the local fields $\mathbf{E}_{loc}$ and $\mathbf{H}_{loc}$. These local fields account for interactions between neighboring dipoles, representing the feedback effect.

Polarizability and array factor are related in the design and behavior of antenna arrays, especially when antennas containing resonant structures or metamaterials are used. The polarizability of individual array elements (whether dipoles, metamaterial elements, or resonators) affects how these elements interact with the electromagnetic field, which in turn influences the radiation pattern of the entire array. In the case of antennas using elements with metamaterials or resonant structures, the polarizability can be highly tuned for certain frequencies, which can modify the radiation behavior of the individual element. Based on basic antenna array theory, the array factor describes how the waves radiated by the individual elements of the antenna array are combined [13]. The polarizability affects the radiation pattern of each element in two ways: in amplitude, if the real part of the polarizability is significant, it can amplify or attenuate the radiated field, and in phase, if the polarizability is complex, its imaginary part introduces an additional phase shift in the emitted wave. The polarizability of each element can be described by the Lorentzian function, commonly used to model resonant responses in metamaterials [14–17]:

$$\alpha_m(\omega) = \frac{F\omega^2}{\omega_0^2 - \omega^2 + j\Gamma\omega} \quad (3)$$

where F is the oscillation force, ω_0 the resonance frequency, and Γ the damping factor. Equation (3) is related to the magnetic dipole moment of the metamaterial element $\vec{m}$ and the local field of the waveguide $\vec{H}_{ref}$. The relationship between each metamaterial element and the reference wave is:

$$\vec{m}_i = \alpha_{m,i}(\omega)\vec{H}(x_i) \quad (4)$$

Using the approximation defined in [12] it is possible to determine the radiation pattern for a one-dimensional array as:

$$AF(\phi,\theta) = \cos\theta \sum_{i=1}^{N} \alpha_{m,i}(\omega) e^{-j\beta x_i} e^{jkx_i sin\phi} \quad (5)$$

To control the radiation contribution of each cell, it is necessary to control the polarizability α_m of each cell near the resonance frequency ω_0. Figure 1 presents the magnitude and phase of the polarizability of a unit cell. Tuning an element can be done by changing its resonance frequency ω_0, causing magnitude and phase changes in the polarizability. Since the polarizability is a complex analytical function of the resonance frequency, magnitude and phase are totally related and present a restriction in the phase advance reducing the control range, as the magnitude decays at the extremes of the resonance frequency. The use of sublambda elements allows to reduce the spaces between elements, and the accumulation of the phase of the guided wave helps to recover the phase control of the elements.

The polarizability of each element is a function that depends on its geometry, resonance, and electromagnetic environment. This mapping involves periodic adjustments in the magnitude of α, resulting in an oscillating modulation profile that contributes to the formation of the major lobe and minor lobes. For beamforming, linearly increasing weights of constant amplitude and phase can be found. Lorentzian Constrained Modulation (LCM) mentioned in [12] is an approach that simultaneously optimizes the phase and magnitude of each metamaterial element in an antenna array.

$$\alpha_{m,i}(\omega) = \frac{j + e^{j(\beta x_i + kx_i sin(\phi_0))}}{2} \quad (6)$$

Equation (6) reflects the combination of a constant component (representing a phase adjustment) and an exponential component $e^{\beta x_i + kx_i n(\phi_0)}$ representing the phase variation as a function of position. $n(\phi_0)$ corresponds to the desired radiation angle ϕ_0. This term indicates how the radiation from each cell contributes to forming the beam in the desired direction ϕ_0.

Recapitulating Equation (5), $\alpha_{mi}(\omega)$ does not fully represent the behavior of LCPHs in a waveguide with a single-port excitation and a metallic termination at the other end (closed circuit). In this configuration, the closed port generates a standing wave inside the waveguide, requiring a different approach

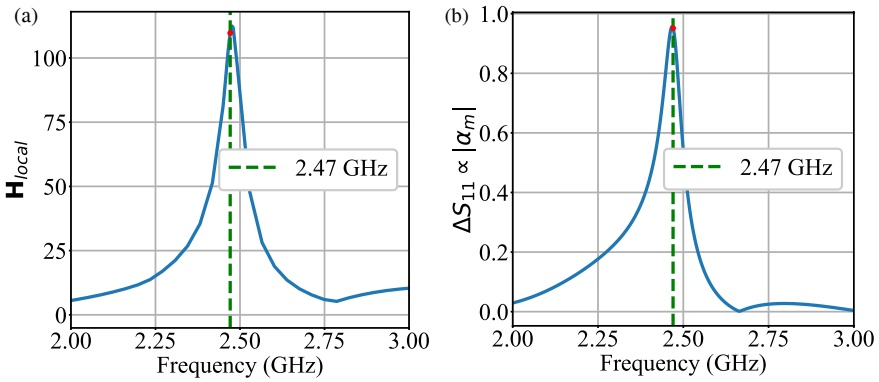

FIGURE 2. Comparison of field response and estimated polarizability for a CELC cell with dimensions 18×18 mm (a) Local magnetic field $\mathbf{H}_{local}$ at the cell position. (b) Calculate magnetic polarizability α_m.

to analyze the cells. For a WR340 waveguide, this standing wave influences how the amplitude and phase of the cells are measured. Additionally, the electromagnetic fields within the waveguide exhibit a sinusoidal spatial distribution, characteristic of the TE_{10} mode.

$$H_z \propto n\left(\frac{\pi x}{a}\right) \tag{7}$$

2.1. Phase and Amplitude Measurement with a Single Port

Even though port 2 is closed, it is possible to measure the amplitude and phase of the cells through indirect measurements from port 1. Parameter S_{11} reflects the effect of the CELC cells and the interaction of the reflected fields at the closed port, and if S_{11} is measured in different configurations (e.g. with the first cell, with the second cell, etc.) the incremental contribution of each cell can be deduced. The approximate calculation of magnitude and phase per cell requires deducing the contribution of each cell from S_{11}. For simplicity, the following model can be used:

$$\Delta S_{11} = S_{11,with\ cells} - S_{11,without\ cells} \tag{8}$$

The amplitude and phase of a cell are related to ΔS_{11} as:

$$A_{cell} = |\Delta S_{11}| \tag{9}$$

$$\phi_{celda} = \arg(\Delta S_{11}) \tag{10}$$

Additionally, when there is a small space, it involves modifying the effective phase of each cell and, in some cases, adjusting the magnetic polarizability to compensate the position mismatch with respect to the magnetic field maxima.

2.2. Polarizability from Incremental Difference Calculation

The definition of magnetic polarizability α_m from incremental difference calculation (ΔS_{11}) comes from the analysis of the fundamental principles of electromagnetic interactions and the properties of metasurfaces. This approach is based on the concepts of local perturbations of an electromagnetic field and how they affect observable properties such as the reflection coefficient [18]. In the case of CELC cells, it acts as a resonator responding to a local magnetic field $\mathbf{H}_{local}$ generating a magnetic dipole moment ($\mathbf{m}$).

$$\mathbf{m} = \alpha_m \mathbf{H}_{local} \tag{11}$$

The polarizability α_m describes the ability of the cell to respond to the $\mathbf{H}_{local}$ field. The relationship with S_{11} occurs when a metamaterial cell is inserted into the waveguide, producing perturbations.

The magnitude of ΔS_{11} is proportional to the induced magnetic dipole moment m, which in turn depends on α_m and $\mathbf{H}_{local}$. Therefore, the polarizability can be deduced as:

$$\alpha_m = \frac{\Delta S_{11}}{\mathbf{H}_{local}} \tag{12}$$

Experimentally, the field H_{local} represents the incident magnetic field at the cell position, which can be measured or estimated by simulation. The incremental reflection coefficient ΔS_{11} is calculated as described in Eq. (8), comparing the system with and without each metamaterial cell. Therefore, the change in magnitude of ΔS_{11} is proportional to the induced dipole moment m.

$$\Delta S_{11} \propto \mathbf{m} \propto \alpha_m \mathbf{H}_{local} \tag{13}$$

Through simulations, the proportionality of the local field can be verified with the incremental calculation, which in turn is proportional to the polarizability as shown in Figure 2.

3. INCREMENTAL METHOD VALIDATION

Based on the characterization provided by the Incremental Difference Method [8], the magnitude and phase response of each metamaterial cell are predicted through individual tuning. The structures are characterized by correlating the resonance frequency with the physical dimensions of the CELC cells [19, 20]. The resonance frequency of each CELC cell is primarily controlled by its geometric dimensions. Increasing the physical size of the resonator elements (e.g., arm length, loop area) results in a lower resonance frequency due to higher effective inductance and capacitance. This behavior enables frequency tuning through dimensional scaling, as illustrated in Figure 3. Since the polarizability of each element follows a Lorentzian profile centered at its resonance frequency, dimen-

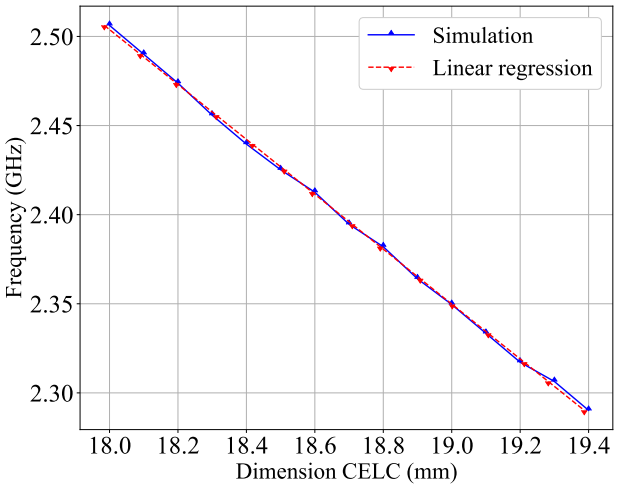

FIGURE 3. Relationship between resonance frequency and the size of the CELC cell. A linear regression is used to determine the optimal dimension for the target frequency.

sion adjustments directly influence both amplitude and phase response, allowing for tailored radiation contributions in the array.

For this design, the waveguide structure is adapted to a practical implementation model using a WR340 waveguide-to-coaxial adapter as the foundation (Figure 4). A conical exciter is employed, and the position of the CELC cells is adjusted along the Z-axis to characterize each structure individually. This allows the extraction of amplitude and phase contributions from each cell. Figure 5 shows the spatial distribution of the cells along the waveguide, with a separation of $\lambda_0/4$ between them. Full-wave characterization is performed at each position x_i. As shown in Figure 5, the amplitude and phase of the magnetic polarizability exhibit the expected Lorentzian behavior as a function of the cell size. The resonance frequency is directly controlled by the geometry of the CELC elements (see Figure 6), which confirms that dimensional tuning leads to frequency shifts consistent with the analytical model. These results support the validity of using the Lorentzian formulation to approximate the near-resonant response of the CELC cells in both amplitude and phase.

To maximize radiative efficiency and ensure the radiation pattern adheres to the amplitude and phase constraints of the CELC cells, we focused on the geometric optimization of the unit cells. By adjusting their dimensions, the resonance frequency of each element was shifted accordingly.

Referring back to Equation (6), we estimate the amplitude and phase distributions of the metamaterial elements along the waveguide. This mapping is performed with respect to the excitation point located at cell CELC2. Phase adjustments are implemented to steer the radiation pattern toward $-30°$ from broadside ($\cos(\theta) = 1$) [12, 13]. However, the amplitude and phase configuration obtained for the elements, as shown in Figure 6, does not fully conform to the expected LCM function. Instead, the direction of the radiation pattern is primarily influenced by the elements with the highest magnetic polarizability, in this case, CRLC1 and CELC4 cells.

As shown in Figure 7, the amplitude responses of CELC1, CELC4, and CELC5 are the closest to those predicted by the LCPH model. Based on the amplitude and phase values obtained using the Incremental Difference Method, the array factor defined in Equation (5) is computed and illustrated in Figure 8, where $\alpha_{m,i}$ represent the discrete magnetic polarizability values assigned to each cell.

Due to the Lorentzian nature of the magnetic polarizability, the available phase shift for each CELC element is limited. As shown in Figure 6(b), the effective phase control range extends from approximately $17°$ to $-130°$, covering about $147°$ around the resonance frequency. Beyond this range, the polarizability amplitude diminishes significantly, reducing the effective contribution to the radiation pattern. This phase variation, while restricted, is sufficient to enable directional beam steering using subwavelength resonators.

Since the magnetic polarizability follows a Lorentzian profile, its magnitude decays sharply at frequencies away from resonance. As a result, the effective contribution of a CELC cell to the radiation pattern is significantly reduced when it operates outside the near-resonant band. Consequently, phase control is only meaningful within a limited frequency range where the polarizability amplitude remains sufficiently high, directly constraining the achievable beam steering performance. This behavior is consistent with the analysis presented in [12], where it is emphasized that significant amplitude and effective phase control in metasurface antennas based on resonant elements occur primarily around the resonance frequency.

4. SIMULATION RESULTS

The simulation results are validated using the 3D model shown in Figure 4 and the conical exciter depicted in Figure 5(b). In the full-wave simulations, the waveguide body and CELC elements were modeled as perfect electric conductors (PECs), accurately approximating the behavior of aluminum at 2.45 GHz. The excitation system, based on a Type-N female connector, was modeled with realistic material properties: the inner conductor and conical transition were assigned aluminum, and the dielectric support was included to match the practical connector structure. This design reflects the fabricated antenna base, where the connector is already installed and ready for experimental validation. Additionally, the structure has been rotated according to the weighting values obtained in Figure 7. It is important to highlight that the weights were adjusted to comply with the amplitude and phase limitations imposed by the CELC cells along the waveguide. Moreover, the theoretical array factor model does not account for the secondary effects introduced by the waveguide structure. To better reflect realistic operating conditions, the simulation incorporates a discrete port, simulating a $50\,\Omega$ impedance at the external connection point of the coaxial cable. The resulting structural dimensions are shown in Figure 9.

The simulations were carried out assuming perfect electric conductors (PECs) for both the waveguide and CELC elements. This is a valid assumption in the WR340 configuration, where all components are metallic. In a practical prototype, the structure would be fabricated using aluminum, a highly conductive

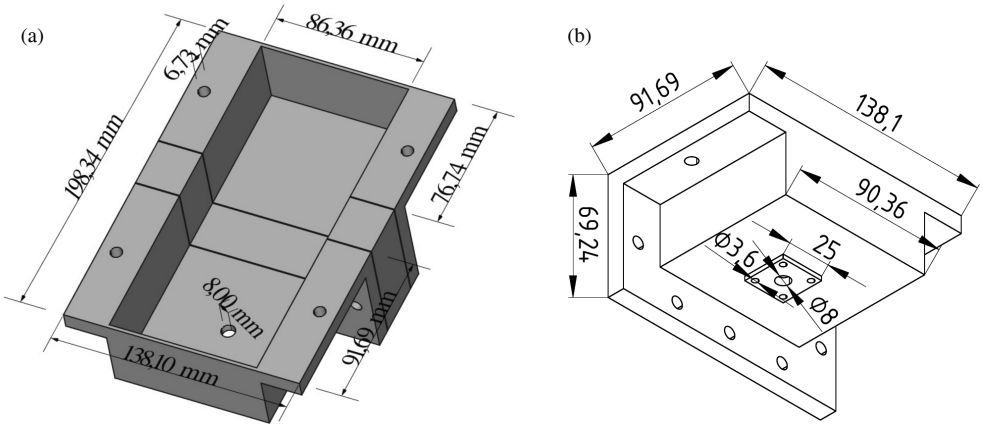

FIGURE 4. 3D model of the metasurface antenna base. (a) Full assembly including three sections: coaxial adapter, separation region, and short-circuited termination. (b) Detail of the waveguide adapter section with dimensions (units in mm.)

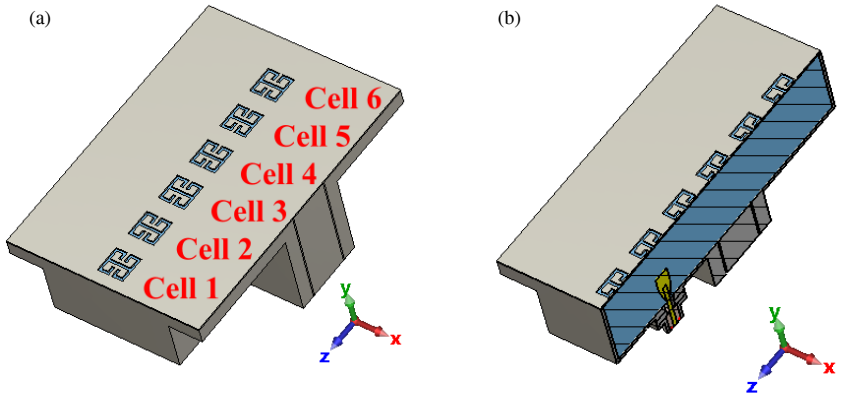

FIGURE 5. Metasurface antenna prototype based on a WR340 waveguide. (a) Distribution of CELC cells with $\lambda_0/4$ spacing along the waveguide. (b) Sectional view showing the position of the conical exciter.

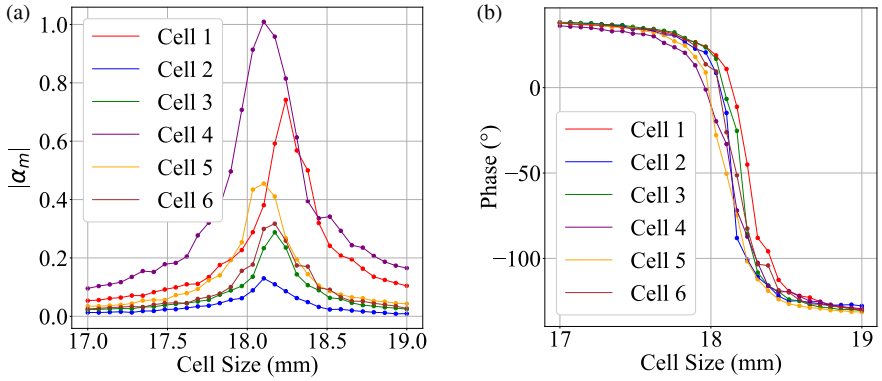

FIGURE 6. Variation of CELC cell polarizability as a function of its geometric dimensions. (a) Magnitude of the magnetic polarizability α_m versus cell size, (b) Phase of the magnetic polarizability $\angle\alpha_m$ versus cell size.

material. Although finite conductivity introduces small ohmic losses, their effect on the amplitude of the magnetic polarizability is minimal. Therefore, the performance obtained from simulations is expected to closely approximate the experimental results.

The short-circuited termination establishes a standing wave pattern inside the waveguide, characterized by sinusoidal variations of the magnetic field along the propagation axis. This standing wave is essential for the operation of the metasurface antenna, as it provides the necessary local magnetic field excitation for the CELC cells distributed along the waveguide. The periodic arrangement of the CELC elements, following a subwavelength distribution as proposed in [12], ensures efficient

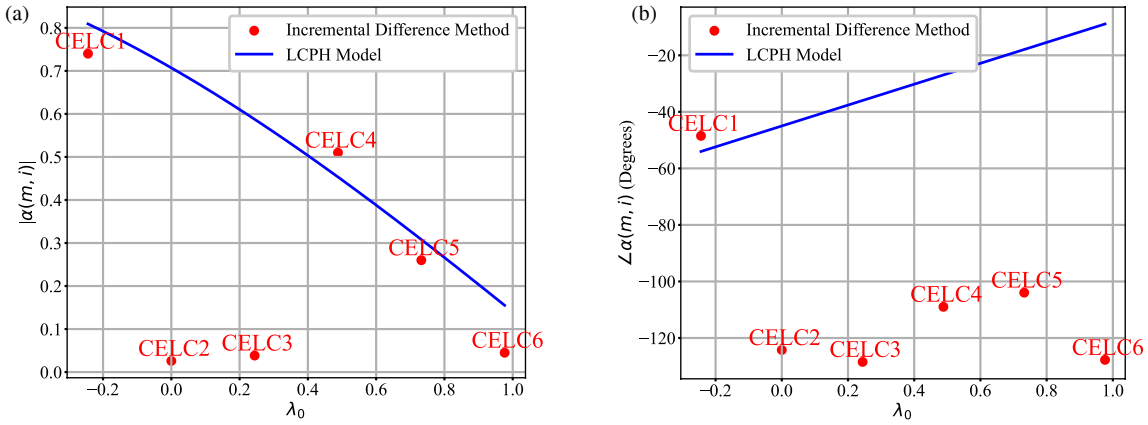

FIGURE 7. Comparison between theoretical models of magnetic polarizability for CELC cells. (a) Amplitude of α_m obtained using the Incremental Difference Method versus the LCPH model. (b) Phase of α_m from both methods.

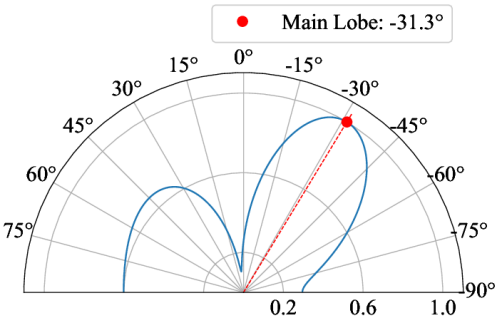

FIGURE 8. Radiation pattern of the metasurface antenna using six CELC cells. Polar plot of the radiation pattern with respect to the broadside direction ($\theta = 0°$), Main lobe oriented at approximately $-30°$

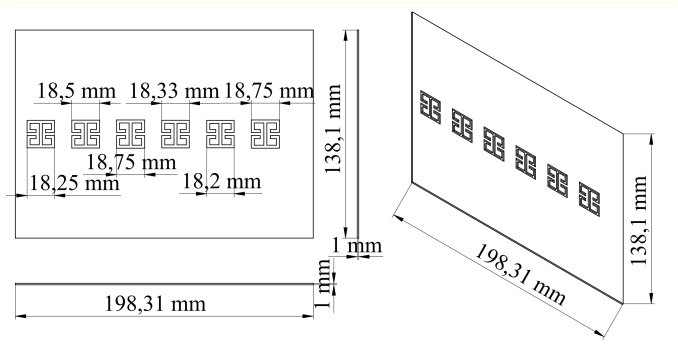

FIGURE 9. Metasurface antenna array designed to steer the main radiation lobe at 30°. CELC cells are spaced by $\lambda_0/4$.

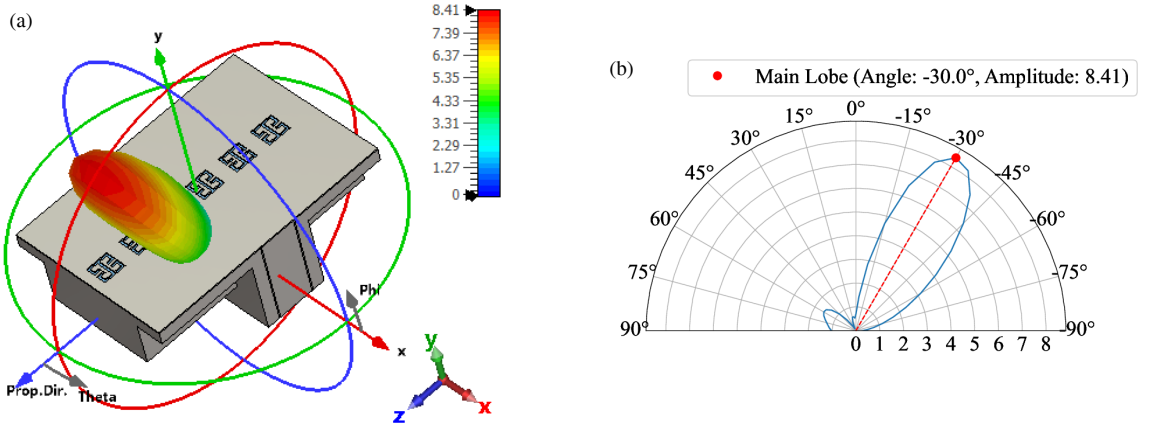

FIGURE 10. Full-wave simulation results for the 6-cell CELC array. (a) 3D radiation diagram showing directional behavior. (b) Elevation plane radiation pattern highlighting beam steering from broadside.

excitation across the array while minimizing mutual coupling effects.

The simulation results are presented in Figure 10, where it is verified that the design and placement of the CELC cells effectively steer the radiation pattern in the desired direction.

Although a $\lambda_0/4$ periodic spacing was employed to reduce the likelihood of grating lobes, the presence of physical constraints on the CELC elements may still lead to secondary lobes, as discussed in [21]. In this design, while no specific grating lobe suppression techniques were implemented, the simulated radiation patterns show relatively low secondary lobe levels.

This behavior is likely attributed to the standing wave field inside the waveguide and the tailored amplitude and phase distribution achieved via the Incremental Difference Method.

In addition to supporting field sampling and beam steering, the $\lambda_0/4$ spacing helps minimize the mutual coupling between adjacent CELC elements. The subwavelength resonant nature of the CELC cells results in weak near-field interaction, ensuring that each element's polarizability remains largely independent. This contributes to preserving the intended amplitude and phase distribution across the metasurface.

5. CONCLUSIONS

This work presents the design and validation of a waveguide-fed metasurface antenna using CELC metamaterial elements. By employing Incremental Difference Method, we obtained a localized estimation of the magnetic polarizability of each unit cell, enabling effective amplitude and phase mapping along the structure. Lorentzian Constrained Phase Hologram (LCPH) model served as a theoretical basis for amplitude-phase weighting, guiding the direction of the radiation pattern.

The simulation results confirm the ability of the CELC-based metasurface to steer the main lobe toward a desired direction, in this case $-30°$, with good agreement between the predicted polarizabilities and resulting field distribution. Furthermore, the full-wave model incorporating realistic waveguide effects demonstrates the practical viability of this approach, despite some limitations due to the inherent phase and amplitude constraints of the metamaterial elements.

Although the LCPH model assumes full control over amplitude and phase for each element, in practice, resonant elements such as CELC cells are constrained by their geometric tuning range. As discussed in [12, 21], analytical profiles can guide the design, but not all cells can simultaneously reach the desired values. Figure 7 shows that only some cells approach the theoretical LCPH behavior. Therefore, the beam was formed using the cells with the closest match to the target polarizability values, while others contributed with limited weight. This design strategy enables beam steering within practical constraints and avoids relying on idealized uniform control assumptions.

While the present work focuses on passive CELC cells with fixed geometrical tuning, dynamic metasurface antennas have been demonstrated using tunable components [22]. Future work will explore the application of Incremental Difference Method to microstrip-based technologies, enabling real-time reconfigurable metasurface designs through the integration of varactors, micro-electromechanical switches (MEMSs), or other tunable devices.

The maximum steering angle achievable with the designed metasurface antenna is constrained by the limited phase range available due to the Lorentzian polarizability behavior, amplitude decay away from resonance, and the standing wave distribution inside the waveguide. While the $\lambda_0/4$ spacing helps maintain control and suppress grating lobes, steering beyond moderate angles would require broader phase control or dynamic tuning mechanisms.

Full-wave simulation results show that the metasurface antenna achieves a main beam with a half-power beamwidth (HPBW) of approximately 40.7°. The secondary lobes, as observed in the radiation pattern, are considerably smaller than the main lobe, demonstrating effective beam steering performance with acceptable side lobe behavior, despite the intrinsic limitations of the resonant CELC elements.

Compared to traditional phased arrays, the waveguide-fed metasurface antenna presented here offers a simpler, lower-cost solution for beam steering, relying on passive subwavelength resonators instead of active phase shifters. While the achievable steering range and dynamic reconfigurability are limited, the approach provides an effective and compact alternative for applications requiring directional radiation control without the complexity of fully active systems.

- Advantages of the proposed design:
  - Simple single-port feeding system.
  - Passive implementation without active phase shifters.
  - Compact and low-profile structure.
  - Demonstrated beam steering using passive subwavelength elements.
- Limitations:
  - Fixed beam direction after fabrication.
  - Limited phase control compared to fully active phased arrays.
  - Real-time reconfigurability not implemented (requires tunable components).

Building on the Lorentzian Constrained Phase Hologram (LCPH) methodology, future work may explore the integration of tunable elements, such as varactors or PIN diodes [23], to enable dynamic beam control. Additionally, the technique could be extended to two-dimensional metasurfaces, where real-time reconfigurability can be investigated by embedding tunable components directly within the CELC structures.

ACKNOWLEDGEMENT

This work was partly supported by Dirección de gestión de recursos para CTel — equipos salud (Convocatoria 844-2019 Ministerio de Ciencia, Tecnología e Innovación, Colombia), project code 130884467291.

REFERENCES

[1] Huang, C., A. Zappone, G. C. Alexandropoulos, M. Debbah, and C. Yuen, "Reconfigurable intelligent surfaces for energy efficiency in wireless communication," *IEEE Transactions on Wireless Communications*, Vol. 18, No. 8, 4157–4170, 2019.

[2] Lin, F. H. and Z. N. Chen, "Low-profile wideband metasurface antennas using characteristic mode analysis," *IEEE Transactions on Antennas and Propagation*, Vol. 65, No. 4, 1706–1713, 2017.

[3] Shamim, S., A. S. M. Mohsin, M. M. Rahman, and M. B. H. Bhuian, "Recent advances in the metamaterial and metasurface-based biosensor in the gigahertz, terahertz, and optical frequency domains," *Heliyon*, Vol. 10, No. 13, e33272, 2024.

[4] Selvaraj, M., R. Vijay, R. Anbazhagan, and A. Rengarajan, "Reconfigurable metasurface: Enabling tunable reflection in 6G wireless communications," *Sensors*, Vol. 23, No. 22, 9166, 2023.

[5] Ashraf, N., T. Saeed, H. Taghvaee, S. Abadal, V. Vassiliou, C. Liaskos, A. Pitsillides, and M. Lestas, "Intelligent beam steering for wireless communication using programmable metasurfaces," *IEEE Transactions on Intelligent Transportation Systems*, Vol. 24, No. 5, 4848–4861, 2023.

[6] Hu, J., G. Q. Luo, and Z.-C. Hao, "A wideband quad-polarization reconfigurable metasurface antenna," *IEEE Access*, Vol. 6, 6130–6137, 2017.

[7] Jian, M., G. C. Alexandropoulos, E. Basar, C. Huang, R. Liu, Y. Liu, and C. Yuen, "Reconfigurable intelligent surfaces for wireless communications: Overview of hardware designs, channel models, and estimation techniques," *Intelligent and Converged Networks*, Vol. 3, No. 1, 1–32, 2022.

[8] Wang, X., J. Q. Han, G. X. Li, D. X. Xia, M. Y. Chang, X. J. Ma, H. Xue, P. Xu, R. J. Li, K. Y. Zhang, *et al.*, "High-performance cost efficient simultaneous wireless information and power transfers deploying jointly modulated amplifying programmable metasurface," *Nature Communications*, Vol. 14, No. 1, 6002, 2023.

[9] Yang, W., J. Li, D. Chen, Y. Cao, Q. Xue, and W. Che, "Advanced metasurface-based antennas: A review," *IEEE Open Journal of Antennas and Propagation*, Vol. 6, No. 1, 6–24, 2025.

[10] Schurig, D., J. J. Mock, and D. R. Smith, "Electric-field-coupled resonators for negative permittivity metamaterials," *Applied Physics Letters*, Vol. 88, No. 4, 041109, 2006.

[11] Hand, T. H., J. Gollub, S. Sajuyigbe, D. R. Smith, and S. A. Cummer, "Characterization of complementary electric field coupled resonant surfaces," *Applied Physics Letters*, Vol. 93, No. 21, 212504, 2008.

[12] Smith, D. R., O. Yurduseven, L. P. Mancera, P. Bowen, and N. B. Kundtz, "Analysis of a waveguide-fed metasurface antenna," *Physical Review Applied*, Vol. 8, No. 5, 054048, Nov. 2017.

[13] Balanis, C. A., *Antenna Theory: Analysis and Design*, John Wiley & Sons, 2016.

[14] Engheta, N. and R. W. Ziolkowski, *Metamaterials: Physics and Engineering Explorations*, John Wiley & Sons, 2006.

[15] Tretyakov, S., *Analytical Modeling in Applied Electromagnetics*, Artech House, 2003.

[16] Pendry, J. B., A. J. Holden, D. J. Robbins, and W. J. Stewart, "Magnetism from conductors and enhanced nonlinear phenomena," *IEEE Transactions on Microwave Theory and Techniques*, Vol. 47, No. 11, 2075–2084, 1999.

[17] Caloz, C. and T. Itoh, *Electromagnetic Metamaterials: Transmission Line Theory and Microwave Applications*, John Wiley & Sons, 2005.

[18] Sakyi, P., J. Dugan, D. Kundu, T. J. Smy, and S. Gupta, "Waveguide-floquet mapping using surface susceptibilities for passive and active metasurface unit cell characterization," *IEEE Transactions on Antennas and Propagation*, Vol. 72, No. 9, 7110–7121, 2024.

[19] Baena, J. D., R. Marqués, F. Medina, and J. Martel, "Artificial magnetic metamaterial design by using spiral resonators," *Physical Review B*, Vol. 69, No. 1, 014402, Jan. 2004.

[20] Baena, J. D., J. Bonache, F. Martín, R. M. Sillero, F. Falcone, T. Lopetegi, M. A. G. Laso, J. Garcia-Garcia, I. Gil, M. F. Portillo, and M. Sorolla, "Equivalent-circuit models for split-ring resonators and complementary split-ring resonators coupled to planar transmission lines," *IEEE Transactions on Microwave Theory and Techniques*, Vol. 53, No. 4, 1451–1461, 2005.

[21] Boyarsky, M., M. F. Imani, and D. R. Smith, "Grating lobe suppression in metasurface antenna arrays with a waveguide feed layer," *Optics Express*, Vol. 28, No. 16, 23 991–24 004, Aug. 2020.

[22] Lin, M., X. Huang, B. Deng, J. Zhang, D. Guan, D. Yu, and Y. Qin, "A high-efficiency reconfigurable element for dynamic metasurface antenna," *IEEE Access*, Vol. 8, 87 446–87 455, 2020.

[23] Sleasman, T., M. F. Imani, W. Xu, J. Hunt, T. Driscoll, M. S. Reynolds, and D. R. Smith, "Waveguide-fed tunable metamaterial element for dynamic apertures," *IEEE Antennas and Wireless Propagation Letters*, Vol. 15, 606–609, 2015.